Proceedings of the 20th International Conference on Soil Mechanics and Geotechnical Engineering– Rahman and Jaksa (Eds)
© 2022 Australian Geomechanics Society, Sydney, Australia, ISBN 978-0-9946261-4-1

Evaluation and monitoring of man-made slope failure at Øysand, Norway

Évaluation et surveillance de la rupture de pente artificielle à Øysand, Norvège

Yunsup Shin, Jung Chan Choi, Santiago Quinteros & Brian Carlton
Norwegian Geotechnical Institute, Sognsveien 72, Oslo, Norway; yunsup.shin@ngi.no

Jean-Sebastien L'Heureux
Norwegian Geotechnical Institute, Trondheim, Norway

Joohyun Seong
Korea Infrastructure Safety and Technology Corporation, JinjuKorea

ABSTRACT: The road and railways infrastructure developments in Norway have increased the interest in the geotechnical challenges associated with slope stability under freezing-thawing cycles. In this case study, a critical slope was identified in a cold region based on field site investigation and frost-heave laboratory tests, and a series of numerical simulations were carried out before creating a man-made slope at Øysand, Norway. A remote monitoring system was installed on the large scaled man-made slope to observe its behavior against the governing factors of slope stability. It was noted that slope stability was slightly impacted by the freezing–thawing action, which was monitored by the initial field observations from November 2019 to March 2020. The slope failed in April 2020 after a heavy precipitation event. Back-calculations of the slope stability were performed to find out the main reason for the slope failure. It was found that the most likely reason was heavy rainfall with intensity over 5 mm/hr, inducing the flux of water through the tension cracks, increasing pore water pressure, and decreasing the matric suction, which resulted in reduction of shear strength and failure of the man-made slope. The slope was minorly impacted by the freezing-thawing action during the observation period.

RÉSUMÉ : Les développements des infrastructures routières et ferroviaires en Norvège ont suscité un intérêt pour les défis géotechniques associés à la stabilité des pentes sous les cycles de gel-dégel. Dans cette étude de cas, une pente critique a été identifiée dans une région froide sur la base d'une enquête sur le terrain et d'essais en laboratoire de soulèvement dû au gel, et une série de simulations numériques a été réalisée avant de créer une pente artificielle à Øysand, en Norvège. Un système de surveillance à distance a été installé sur la pente artificielle à grande échelle pour observer son comportement par rapport aux facteurs déterminants de la stabilité de la pente. Il a été noté que la stabilité de la pente a été légèrement affectée par l'action de gel-dégel, qui a été surveillée par les observations initiales sur le terrain de novembre 2019 à mars 2020. Après la rupture de la pente en avril 2020, les calculs à rebours de la stabilité de la pente ont été effectués. pour découvrir une raison principale de la rupture de la pente. Il a été constaté que la principale raison attendue de l'échec est une forte pluie de plus de 5 mm/h d'intensité induisant le flux d'eau à travers les fissures de tension, augmentant la pression de l'eau interstitielle et diminuant la succion matricielle, la pente artificielle a échoué. La pente a été légèrement affectée par l'action de gel-dégel pendant la période d'observation.

KEYWORDS: slope stability; monitoring; freezing–thawing; cold region; back-calculation

1 INTRODUCTION

Recent infrastructure developments of road and railways networks in Norway have led to increased interest in the geotechnical challenges associated with slope stability under freezing–thawing cycles. The freezing–thawing cycles may cause slope instability due to soil deformation and strength reduction (Zwissler, B., et al., 2014; Heidari, M., et al., 2017; Yilmaz, F., et al., 2018).

When saturated fine-grained soil is subjected to freezing temperatures below 0 °C, part of the water in the soil voids is frozen to ice. A film of unfrozen water close to the frozen soil particles is absorbed into the ice and forms ice lenses. In this process, water is sucked up from the unfrozen soil void developing a gradient in the water potential in the same direction as the temperature gradient (Chamberlain, E.J., et al., 1978). Once freezing stops, due to the air temperature above 0 °C, the thawing process from the ground surface begins. During thawing, water escapes easily through the spaces formerly occupied by the ice, leaving the void empty and leading to high compressibility and low soil strength (Graham, J., et al., 1985). These freezing–thawing cycles can significantly impact the stability of a slope. The impact of freezing–thawing on the stability of slopes has been studied by numerical simulations using, e.g., coupled thermal–hydraulic–mechanical models (Korshunov, A. A., et al., 2016). Such numerical research concluded that freezing of the soil on the slope increases its volume by attracting water from the groundwater table, while thawing reduces the effective soil strength by increasing hydraulic gradients, which can lead to slope failure (Andersland, 2004). To prevent slope failure, slope monitoring practices typically involve the periodic measurement of the slope condition by scanning the slope surface to identify and quantify the nature and extent of pit slope movements (Harries, N.J., et al., 2007). Field monitoring techniques may also include devices that measure matric suction and volumetric water content (Pirone, M., et al., 2014).

In this study, an unstable slope area was identified by an initial screening, and the field monitoring on the slope was performed to monitor the behaviour of the test slope subjected to freezing–thawing cycles and heavy rainfall over the year. The slope behavior was back-calculated based on the slope failure to evaluate the governing factor influencing the slope stability.

2 SITE INVESTIGATION

Site investigations including cone penetration tests (CPTu) and sampling were performed in 2017 and 2019 in the test area. The locations of the site investigation are presented in Figure 1.

For the first phase, two total sounding, TS (OYSTS05 and OYSTS07) and one CPTu (OYSC07) were performed on the top of the slope. Additional TS (OYSTS09) and C PTu (OYSC02) at the bottom of the slope were done in t he second phase. CPTu and TS are used for the identificat ion of the main soil layers. CPTu is also used to derive s oil strength parameters, which are used for slope stability analysis. (OYS: Øysand site, TS: total sounding, C: CPT).

Figure 2 shows the CPTu results in terms of cone resis tance (q_c), sleeve friction (f_s), and pore water pressure (u_2) . The zero depth is fixed at the top of the slope, hence th e depth of OYSC02 (performed at the bottom of the slope) was corrected by adding 6.1 m to the measured depth in the field. A surficial silty sandy layer is identified in the very first meter of the slope, while clayey, silty soil was f ound from 2 m to about 5.5 m depth. The clay content se emed to increase with depth because the pore water pressu re u2 increased between 3.5 and 5.5 m. Below 5.5 m and down to about 10 m depth, interlayered gravelly sand and gravels were found. Below that depth and down to 20 m,

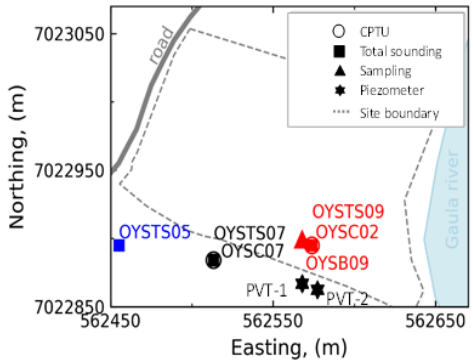

sandy silty and gravelly sands were found.

Figure 1. Location map of the field tests at Øysand Trondheim, Norway

In general, the stratigraphy down to a depth of 10 m from the top of the slope can be divided into two main units: (a) A top 6 m of clayey silt and silty soils and (b) a lower unit of deposited gravelly sand and gravels. The level of the groundwater table was identified by plotting the hydrostatic pore pressure (kPa) versus the depth (m) of the piezometer readings. A correction was applied to the pressure measured by the piezometer, namely by subtracting the piezometer to the air-pressure obtained from a nearby installed weather station. The groundwater level from two piezometers is estimated to be about 2 m from the slope surface.

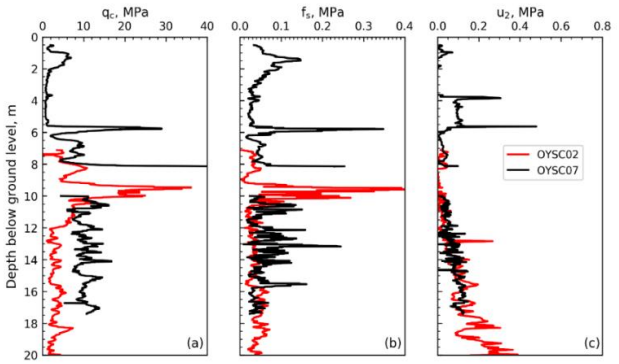

Figure 2. Cone penetration tests (CPTu)s at the test site (a) cone resistance, (b) shaft friction, and (c) pore water pressure

3 MAN-MADE TEST SLOPE

3.1 *Unstable slope identification*

An initial screening over the area of the test site was performed to identify the stability of slope using an in-house computer program (Carlton et al., 2017).

This tool is used to define the most critical profiles for more advanced slope stability analysis. The program discretises the three-dimensional topographic and soil properties data into equally sized blocks.

For blocks on the soil surface, the program calculates the slope angle as the angle between the highest and lowest edge points of the surface face. Blocks below the surface take the slope angle of the block directly above. The program then performs one-dimensional (1D) infinite static and pseudo-static slope stability analyses, First Order Second Moment (FOSM) probabilistic analyses, and simplified seismic displacement analyses to estimate the factor of safety, probability of failure, and seismically induced permanent displacements for each soil block.

Figure 3 shows the topography and slope angle for the area around the selected slope. The elevation varies between 0 at the river surface and 12 meters maximum. In general, the slope angles are between 0 and 3 degrees, except at the selected slope and next to the river, where slope angles as high as 30 degrees are present. Figure 4 presents the static factor of safety and maximum probability of the static FoS < 1 for a slip surface at 10 meters depth. On the steep slopes, the static factor of safety is less than 1.2 and the calculated probability of failure is greater than 63%.

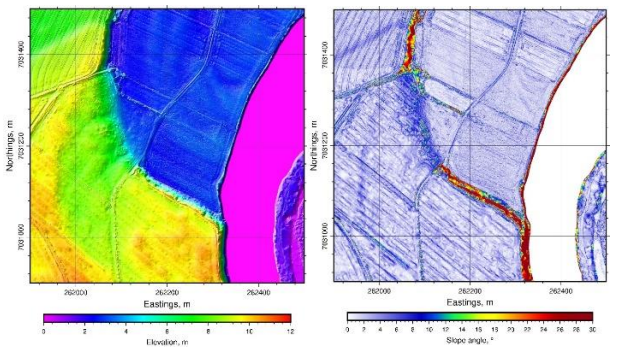

Figure 3 Topography (left) and slope angle (right) for Øysand slope area, Trondheim

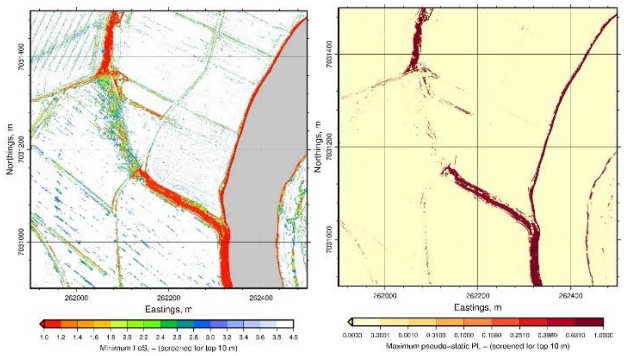

Figure 4 Minimum factor of safety (left) and maximum probability of the static FoS < 1 (right) for Øysand slope area, Trondheim, Norway

3.2 *Grain size distribution*

Representative grain size distribution (GSD) curves obtained from samples at the test site are presented in Figure 5. Samples were collected at the top of the slope, at about 2 m below the top of the slope, at around 5 m downwards, and at the bottom of the

slope. GSDs are useful for preliminary assessment of the frost-heave susceptibility of the soils at Øysand. Soils found on the slope were classified as CL-ML (top to 5 m below) and as SW at the bottom of the slope by American Society for Testing and Materials classification system (ASTM, 2017). Those soils are expected to be highly frost-susceptible based on the Norwegian frost classification system NS200 (Statens Vegvesens, 2014). Frost heave tests were performed on the main soils (ML and SW) to confirm the frost susceptibility of the soils found at the slope surface, results are subsequently presented.

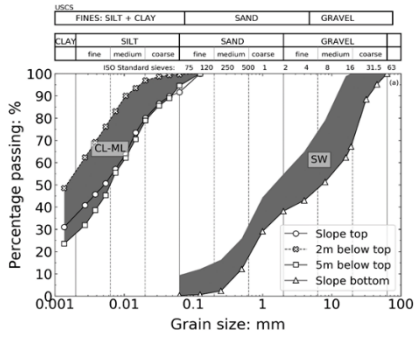

Figure 5. Representative grain size distributions from the slope surface

3.2 *Frost-Heave Tests*

Using a one-dimensional temperature controllable cell, frost-heave expansion of the two soils at the soil slope were investigated, namely ML and SW.

The temperature controllable cell was developed by the Korean Geotechnical Research Institute (KICT, Korea) and slightly modified by NGI (Jin, 2019). The soil was reconstituted following Ishihara (1996) air pluviation by funneling. The specimen height target was 100 mm and the diameter of the cell was 99.72 mm. A relative density of 80% for the SW soil, and a unit weight of 18 kN/m^3 for the ML soil were achieved by tamping. The specimens were then saturated with de-aired water using a small hydrostatic gradient. Finally, freezing was achieved by setting the temperature of the thermostat controlling the bottom cap at −10 °C, the thermostat controlling the temperature of the cell at 1 °C, and the temperature of the top cap at 3 °C. Hence the temperature gradient imposed was 0.13 °C/mm, which is in agreement with the recommendation with the Transport and Road Research Laboratory standard (TRRL) in the UK (Croney, 1967). The vertical effective stresses σ'_v applied to the soil (due to the own weight of the top cap and half of the soil) was 2 kPa.

The experimental results are presented in Figure 6 in terms of the elapsed time after the start of freezing versus the frost-heave expansion as axial strain (ε_a). Experimental results confirmed the suspicion that Øysand soils on the slope face are frost susceptible. The ML soil expansion is about ε_a = 12%, and four times higher than the frost heave expansion of the SW soil (ε_a = 3%).

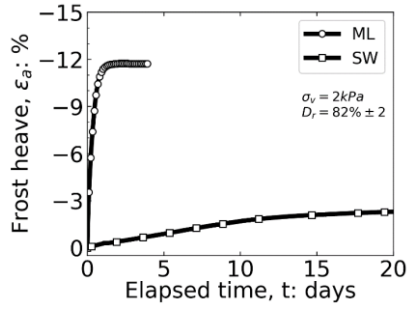

Figure 6 Frost heave results on ML and SW soils from the Øysand site.

3.4 *Man-made test slope*

Based on the identification of unstable slope and the frost-heave tests, the critical slope in the Øysand area was selected for the detail analyses and field monitoring. The critical slope had a dense vegetation cover with large trees and plants, and the slope angle varied between 28° at the top to 34° near the foot. The vegetation cover was removed using an excavator on a 15 m width and 10 m height of the slope. The angle of the slope was reconfigured with a constant gradient of 37° as shown in Figure 7. Soil profile of the slope is composed of slity clay at top 7 m and a sand layer at the bottom of the slope. This man-made slope at Øysand site is located at 63.329097°N and 10.250308°E in Trondheim, Norway.

Figure 7. Man-made test slope at Øysand Trondheim Norway

4 INSTRUMENTATION AND MONITORING

4.1 *Installation of sensors*

The remote monitoring instruments used consisted of: PVT piezometers to monitor changes of the groundwater table with built-in temperature sensor, inclinometers (installed on the middle of the slope) to monitor slope deformations, dielectric water potential sensors, Decagon MPS-6 (Decagon devices, 2017), see Figure 8.

The global deformations of the slope were assessed by Radar/Lidar system. Some of these instruments were connected to a programmed datalogger with a data transfer unit, see Figure 8c. The readings were sent to NGI offices using wireless wi-fi router.

A good understanding of the causes of slope failure in a cold region is essential to make a proper monitoring plan. In a cold region, the governing factors of slope failure are severe weather conditions, freezing–thawing effects on the slope, an increase of water content, pore pressure, and the rising of groundwater table. The slope stability monitoring should be designed to measure and detect those factors effectively. The following sensors were selected for slope stability monitoring at the identified critical slope, see Table 1:

Table 1. Planning of sensors on the slope at Øysand

Sensors	No. of sensors	ID	Depth m	Locations
PVT (Piezometer)	4	P-1	4.5	Top of the slope
		P-2	8.55	Top of the slope
		P-3	5	Bottom of the slope
		P-4	3	Bottom of the slope
Temperature sensors (PVT)	4	P-1	4.5	Top of the slope
		P-2	8.55	Top of the slope
		P-3	5	Bottom of the slope
		P-4	3	Bottom of the slope
Integrated sensor pack (wc, temparature, tilt)	2	I-1	1	Top of the slope
		I-2	2	Halfway down the slope
Suction sensors (MPS-6)	10	S-1, S-2	0.25, 0.5	Three-quarters of the way down the slope
		S-3, S-4	0.5, 0.25	Halfway down the slope
		S-5, S-6	0.5	Westernmost hole at the top of the slope
		S-7, S-8	0.7	Centre hole at the top of the slope
		S-9, S-0	1.05	Easternmost hole at top of the slope
Lidar/Radar	1 set	-	-	10 m distance at the bottom
Air temperature, hygrometer	1 set	-	-	Top of the slope
Precipitation measure	1 set	-	-	Top of the slope

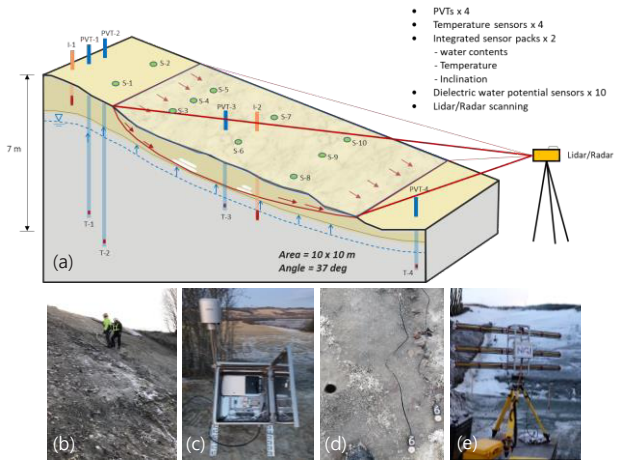

Figure 8. Test slope at Øysand Trondheim Norway: (a) layout of sensor locations; (b) inclinometer installation on 37 degree man-made test slope; (c) data logger box at top of the slope; (d) MPS-6 sensors; (e) Lidar system.

Integrated sensor packs, including water content sensors, temperature sensors, and inclinometers, were placed at two locations. The dielectric water potential sensors with temperature sensors were installed at five locations. The range of soil suction is −9 to −100 kPa, resolution was 0.1 kPa, and accuracy was ± 10% of reading +2kPa from −9 to −100 kPa. The temperature range was −40 °C to 60 °C (resolution 0.1 °C, accuracy ± 1 °C). Radar was set up to scan the images of the slope surface to provide the changes in slope surface geometry. The scanned images can be investigated in connection with the inclinometer data and pore pressure changes, which can be implemented to provide a slope warning system and be used for setting out threshold value(s).

4.2 *Measured data*

Measured pore water pressure and ground temperature from PVTs are presented in Figure 9.

PVT-1 and PVT-2 were embedded at 4.5 m (Unit I, silty clay) and 8.55 m (Unit II, sand) depth (PVT-3 and 4 are to be installed). Measured pore water pressure at PVT-1 was on average 21 kPa, indicating the groundwater level was about 2 m from the slope surface. This was supported by CPT data. Measured pore water pressure at PVT-1 increased from 15 kPa to 27 kPa, proportional to the decrease of ground temperature from 4.2°C to 2°C from November 2019 to January 2020. It is estimated that the frozen ground absorbs unfrozen water, developing a gradient of water in the same direction as the temperature gradient, which can increase the level of the groundwater table. Another reason for the pore pressure increase is the increase of precipitation in this period according to the recorded data from the weather station (NRK Meteorologisk institutt, Øysand, Norway, 2020). Pore water pressure at PVT-2 measured around 15 kPa in early October converged to less than 5 kPa because the pore pressure was dissipated after heavy rain in September at the depth of the gravelly sand of Unit II. Measured temperature from PVT-1 decreased and converged to 2 °C at 4.5 m depth while the temperature from PVT-2 remained constant of 5°C at a depth of 8.55 m.

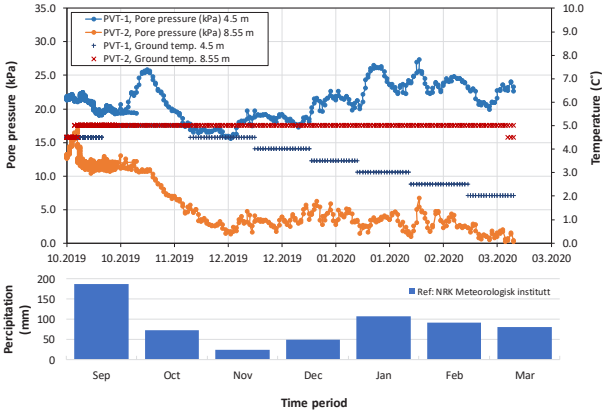

Figure 9. Measured pore water pressure and ground temperature by PVT 1 and PVT 2.

Another measured dataset from the integrated sensor pack I-1 shows the slope inclination, ground temperature, together with air temperature and humidity obtained from November 2019 to March 2020 (Figure 10). Air temperature fluctuated between −12 to +18 °C. Those values were slightly higher than the average temperature in 2017 and 2018 used in the parametric study. Meanwhile, ground temperature was almost constant, ranging from 1.8 to 2 °C at 1.0 m below the surface from the ground. Air humidity varied between 30 to 100%. The values of slope inclination were recorded every hour. The inclination of the slope increased slightly from 0.2° to 0.45°, which meant 2 mm displacement in a downward direction.

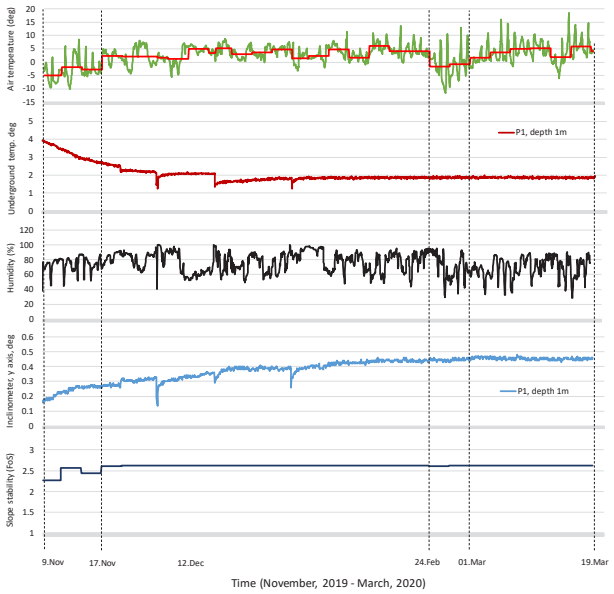

Figure 10. Measured data by sensors on the slope; PVT 1 and PVT 2

Even though this change of inclination is negligible, it is important to keep monitoring the inclination of the slope depending on the changes of ground temperature. A threshold inclination was set to increase the interval of logging of inclinometer data from 1 h to every 10 min.

4.3 *Back-calculation (Oct.2019 to Mar.2020): before slope failure*

The slope stability analysis for the man-made slope was carried out applying the measured data from October 2019 to March 2020, i.e. pore pressure, groundwater table, air and ground temperature, to evaluate a change of stability with time. The average air temperature for 3 days was applied from November to March in Figure 10.

Soil layers are divided into three layers based on the site investigation and observation during excavation. Unit I is the top 1 m soil. It is recognized that desiccation from the surface of clay can cause consolidation and shrinkage in this Unit. Unit II is a silty clay layer with some sand at a depth of 7 m from the top of the slope and Unit III is a sandy gravel layer. The groundwater table was set at 2 m below the ground, as measured by the piezometers. The initial excess pore pressure was activated by total water heads, and the drainage boundary condition was set on the surface of the slope to ensure zero pressure on the surface of the slope and soil remaining saturated. The temperature boundary condition was applied on the surface of the ground.

The full thermal model (TEMP/W) was applied to simulate ground temperature distribution along with the depth, and the saturated/unsaturated model (SEEP/W) was applied to simulate water flow into the soils (Geostudio, 2021). The average air temperature for 3 days was applied to the surface of the ground because the ground temperature was not changed immediately as the air temperature changes. The boundary at the slope surface was modeled with temperature, which is supposed to be transmitted to the ground corresponding to the measured temperature. Coupled seepage analysis was carried out to model groundwater table and pore water pressure, which are matching to the measured pore pressure. The input parameters used for the slope stability analyses have been verified by measured data.

The factors of safety of slope stability were calculated to be in the range of 2.24 to 2.61 from November 2019 to March 2020, considering the measured pore water pressure, groundwater table, air, and ground temperature (Figure 10). In a short period, the factor of safety does not change dramatically depending on the temperature changes in the air because the ground temperature was slowly affected by temperature transmission. But it is necessary to observe the slope behavior, i.e., pore water pressure, ground temperature, inclination, soil suction and surface movement, over the year by the installed monitoring system. Those measured data can be used to update soil parameters and provide much of the information necessary to monitor slope behavior for mitigation and remediation.

4.4 *Back-calculation (April.2020): slope failure*

First signs of failure of the man-made slope were observed in April 2020 (Figure 12). Several tension cracks appeared at the top of the slope and a large crown crack propagated from the top of the slope. The main reason for the slope failure was not the freezing-thawing effect, but a heavy precipitation event. According to the measured data and weather station statistics (NRK Meteorologist Institute, 2020), the precipitation in April was highest during the year 2020, recording 300% higher than the average level of precipitation. Higher than 120 mm precipitation during April at 5 mm/hr rainfall intensity was occurred.

Figure 11. Man-made slope in Øysand site before (left) and after failure (right, April 2020)

The slope factor of safety was back-calculated considering different rainfall intensities to find out the main reason for the slope failure. Figure 12 shows the pore water pressure distribution and the factor of safety by coupled analysis considering measured rainfall intensity of 5 mm/hr versus time. Figure 13 presents the factor of safety versus time after 24 hrs (left) and 5 days (right) with the different rainfall intensities. The suction strength is defined by the following equation (Fredlund et al., 1978):

$$\tau = c' + (\sigma_n - u_a)\tan\phi' + (u_a - u_w)\tan\phi^b$$

where τ is the shear strength; c' the effective cohesion; σ_n the total normal stress; u_a the air pore-air pressure; u_w the pore-water pressure; $(u_a - u_w)$ the matric suction; ϕ' the friction angle; ϕ^b the angle linking the rate of increase in shear strength with increasing matric suction.

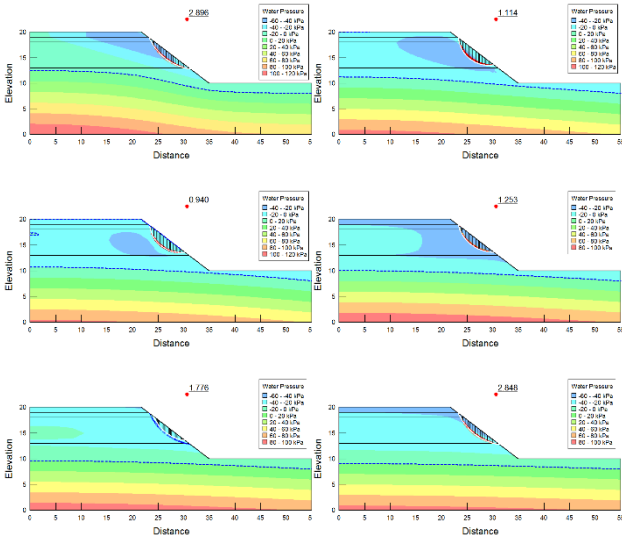

Figure 11. Pore water pressure distribution and FOS by coupled analysis considering rainfall intensity versus time: (a) after 1 hr with a rainfall intensity of 5 mm/hr; (b) 12 hr; (c) 24 hr; (d) 2 days; (e) 3 days; (f) 5 days

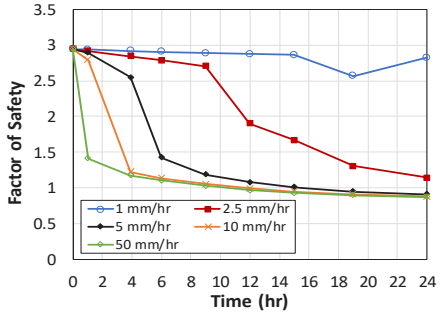

Figure 12. Comparison of factor of safety for the different rainfall intensities for 1day

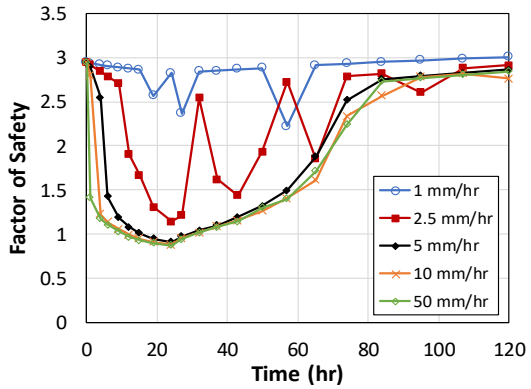

Figure 13. Comparison of factor of safety for the different rainfall intensities for 5 days

In a short period, the factor of safety decreases by a rainfall event. The reduction of the factor of safety is more precipitous and larger for the higher rainfall intensity than the lower rainfall intensity, as shown in Figure 13. As the results of the back-calculation, the factor of safety decreases below 1.0 after 24 hrs with a rainfall intensity greater than 5 mm/hr.

Therefore, the following mechanism for slope failure is postulated. Several small tension cracks were developed 1 m below the top of the slope at the thawing season. From April, higher than normal rainfall increased the flux of water from the ground through the tension cracks, increasing the pore water pressure. The increased pore water pressure reduced the matric suction, developing deeper crown cracks. The factor of safety dropped below 1.0, resulting in the failure of the man-made slope. From the shape of the slope failure (Figure 11), it is noted that the failure of the slope was triggered 1 m below from the top of the slope because of the desiccated top soil and some vegetations. Based on the back-calculations, the factor of safety was recovered after some time following the rainfall events in Figure 13.

5 CONCLUSIONS

For a man-made slope in a cold region, a practical monitoring system has been established to measure and observe slope behavior, i.e. pore pressure, air and ground temperature, inclination, and surface displacement. Slope stability analyses were performed with the measured data to evaluate factors of safety during the winter season from November 2019 to March 2020. After the slope failure in April 2020, the slope stability was back-calculated to find out a main reason of the slope failure. As a result, it was found that:

1. Measured pore water pressure underground increases proportionally to the decrease of ground temperature. It is explained that the frozen ground absorbs unfrozen water, developing a gradient in the water potential in the same direction as the temperature gradient and forming ice lenses, which can cause soil heaving. The frozen ground might increase the level of the groundwater table, but the ice lenses were not formed because the temperature was often fluctuating above and below 0 °C.

2. Measured ground temperature from PVT agreed with the temperature of the integrated sensor pack showing 2–4 °C at 1–4 m depth from the ground surface, while the ground temperature at 8.55 m depth remained constant of 5 °C. It means that the ground temperature deeper than 8 m from the surface remains constant and is not influenced by the change of temperature in the air.

3. Slope stability analyses versus time were performed, taking the measured pore pressure and ground temperature into account. Full thermal and saturated/unsaturated models were applied to simulate ground temperature distribution and water flow into the soils. The factors of safety of the man-made slope from November to March were calculated, ranging between 2.24 to 2.61. The slope stability in a cold region is affected by the weather condition, i.e., freezing–thawing action and precipitation, and this phenomenon should be continuously monitored over the years by an installed monitoring system.

4. After the slope failure, the back-calculations of the slope stability were done to find out a main reason for the failure. The expected reason is that a rainfall event with intensity greater than 5 mm/hr increased the flux of water from the ground, increasing the pore water pressure and decreasing the matric suction. The man-made slope failed as the factor of safety dropped below 1.0.

6 ACKNOWLEDGEMENTS

This research was funded by KISTEC (KAIA project number: 18CTAP-C145146-01). The authors would like to thank KISTEC and the Norwegian GeoTest Sites. for access to the Øysand research site.

7 REFERENCES

ASTM D2487-17. Standard Practice for Classification of Soils for Engineering Purposes, Unified Soil Classification System; ASTM International: West Conshohocken, PA, USA, 2017.

Carlton, B.D., Price, K., Vanneste, M., and Forsberg, C.F. (2017). Development and application of a slope stability assessment screening tool. Proceedings 2nd International Workshop on Landslides in Sensitive Clays, Trondheim, Norway, June 12-14.

Chamberlain, E.J.; Gow, A.J. Effect of freezing and thawing on the permeability and structure of soils. In Proceedings of the International Symposium on Ground Freezing, Bochum, Germany, 8–10 March 1978.

Croney, D.; Jacobs, J.C. The frost susceptibility of soils and road materials. Nat. Acad. Sci. Eng. Med. 1967.

Geostudio. An Engineering Methodology. Available online: http://www.geo-slope.com (accessed on 20 May. 2021)

Graham, J.; Au, V.C.S. Effects of freeze–thaw and softening on a natural clay at low stresses. Can. Geotech. J. 1985, 22, 69–78.

Heidari, M.; Torabi-Kaveh, M.; Mohseni, H. Assessment of the effects of freeze-thaw and salt crystallization ageing tests on Anahita temple stone, Kangavar, west of Iran. Geotech. Geol. Eng. 2017, 35, 121–136, doi:10.1007/s10706-016-0090-y.

Harries, N.J.; Robert, H. The use of slope stability radar (SSR) In Managing SLOPE Instability Hazards in American Rock Mechanics Association, Proceedings of the 1st Canada–US Rock Mechanics Symposium, Vancouver, Canada, 27–31 May 2007

Ishihara, K. Soil Behaviour in Earthquake Geotechnics; Clarendon Press: Oxford, UK, 1996.

Korshunov, A.A.; Doroshenko, S.P.; Nevzorov, A.L. The Impact of Freezing-thawing Process on Slope Stability of Earth Structure in Cold Climate. In Proceedings of the 3rd International Conference on Transportation Geotechnics, Guimaraes, Portugal, 4–7 September 2016; Volume 143, pp. 682–688.

NRK: https://www.yr.no/en/statistics (accessed on 20 April. 2020).

Pirone, M.; Papa, R.; Nicotera, M.V.; Urciuoli, G. In situ monitoring of the groundwater field in an unsaturated pyroclastic slope for slope stability evaluation. Landslides 2014, 12, 259–276, doi:10.1007/s10346-014-0483-z.

Statens Vegvesens. Vegbygging Håndbok N200; Statens Vegvesens: Oslo, Norway, 2014.

Yilmaz, F.; Fidan, D. Influence of freeze-thaw on strength of clayey soil stabilized with lime and perlite. Geomech. Eng. 2018, 14, 301–306, doi:10.12989/gae.2018.14.3.301.

Zwissler, B.; Oommen, T.; Vitton, S. A study of the impacts of freeze-thaw on cliff recession at the Calvert cliffs in Calvert county, Maryland. Geotech. Geol. Eng. 2014, 32, 1133–1148, doi:10.1007/s10706-014-9792-1.